



Long-term irradiation of an ATLAS NSW SM2 Micromegas quadruplet using an AmBe neutron source

Fabian Vogel*, Otmar Biebel, Ralf Hertenberger, on behalf of the ATLAS Muon System

LMU, Am Coulombwall 1, 85748 Garching, Bavaria, Germany

ARTICLE INFO

Keywords:

ATLAS
Micromegas
Longevity
Ageing
Neutron irradiation

ABSTRACT

The NSW Micromegas chambers in the ATLAS forward muon spectrometer are subject to background rates of 15–20 kHz/cm² under HL-LHC conditions. The innermost detector area closest to the LHC beam pipe will accumulate a charge of 0.068 C cm⁻² year⁻¹ under these rates. Due to the late change of the detector gas from non-aging Ar:CO₂ 93:7 vol% to the more HV stable ternary mixture Ar:CO₂:iC₄H₁₀ 93:5:2 vol% and the known vulnerability of wire chambers to Hydrocarbon-containing gas mixtures a three-year-long aging study has been performed. An SM2 series module of the NSW Micromegas quadruplets was irradiated at LMU in Garching/Munich using a 10 GBq AmBe neutron source emitting 6×10^5 MeV n/s as well as 3.5×10^5 4.4 MeV gammas/s and 3.6×10^9 60 keV gammas/s. The SM2 chamber was irradiated in a region of several 10 cm² in size with a dose rate well exceeding the HL-LHC equivalent local charge densities for three years. In between the irradiation periods the performance of the SM2 chamber regarding spatial resolution and efficiency on cosmic muon tracking was tested several times. We report on the irradiation and the performance studies of the SM2 Micromegas quadruplet and conclude that no sign of loss in performance has been observed in contradiction to an earlier experience using drift tube wire chambers.

1. Motivation

Micromegas detectors [1] are a cost-effective device used for tracking Minimum Ionizing Particles over large areas. Small-area Micromegas detectors have been extensively tested and their performance is well understood, providing a spatial resolution of better than 80 μm [2]. Square-meter-sized, resistive strip Micromegas detectors showed high-voltage stability issues and insufficient discharge quenching [3]. To address this, an admixture of isobutane has been added to the commonly used operating gas (Ar:CO₂, 93:7 vol%) to form a ternary gas mixture of Ar:CO₂:iC₄H₁₀ (93:5:2 vol%).

Changing the operating gas resulted in the need for longevity tests. Therefore, a long-term irradiation of a large-area Micromegas detector with neutrons and gammas has been performed over three years. This investigation aimed to gain insights into the behavior and performance of Micromegas detectors under prolonged exposure to radiation focusing on irradiation current development and muon detection efficiency.

2. Irradiation setup

An Americium–Beryllium source was chosen for irradiation. At the start of the irradiation period a source with an activity of 3.7 GBq was

used which was replaced after the first year of irradiation by a 10 GBq source. The 10 GBq AmBe source yields 6×10^5 MeV n/s isotropically [4]. Additionally 3.6×10^9 60 keV gammas [5] and 3.5×10^5 4.4 MeV gammas (see [6,7]) are emitted per second.

For the long-term irradiation the AmBe source was placed in front of the detector touching its outer surface (see Fig. 1). The detector is a spare module of type SM2, identical to the detectors installed in ATLAS consisting of four stacked active volumes [2]. In the following the readout layer closest to the source is also called Layer 1. For the other three layers, the numbering follows with Layer 2, Layer 3, and Layer 4 increasing in distance from the source. Only a part of the detector surface was irradiated. The irradiation strength is discussed in Section 3.

3. Source calibration

The irradiation of the detector surface is inhomogeneous. The source intensity decreases with $1/r^2$, with r being the radial distance from the source. Important to note is the cylindrical source has a finite size ($D = 6$ mm and $L = 15$ mm) and cannot be assumed to be point-like. The distance $|\vec{r}|^2$ depends on the starting point inside the source as sketched in Fig. 2 and Fig. 3.

* Corresponding author.

E-mail address: Fabian.Vogel@physik.uni-muenchen.de (F. Vogel).

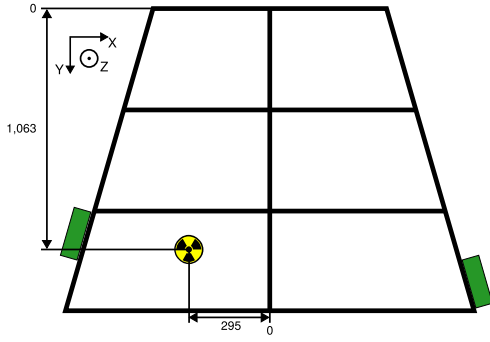


Fig. 1. Sketch of the AmBe source position in front of the Micromegas detector. The detector module is kept in a vertical position. This setup was kept for almost three years testing the detector with the different gas mixtures. The green squares indicate the position of the readout electronics boards. Dimensions are given in mm.

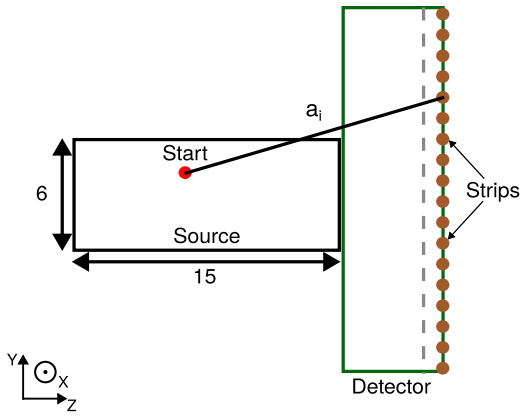


Fig. 2. Side view of the irradiation setup. The source cannot be assumed point-like, hence the starting position of the particle is assumed to be homogeneous within the source volume. The distance from the starting point to the readout strip in the $y-z$ plane is given by a_i for the i th strip. Dimensions are given in mm.

The radial distance $|\vec{r}_i|^2$ is given in the cartesian coordinate system by:

$$|\vec{r}_i|^2 = |\vec{a}_i|^2 + |\vec{x}_i|^2 \quad (1)$$

with x_i being the position along the readout strips and a_i the distance from the starting point in the source to the anode. For the intensity $I(\vec{r})$ follows then:

$$I(\vec{r}) \propto \frac{1}{|\vec{a}_i|^2 + |\vec{x}_i|^2} \quad (2)$$

Since the charges induce the current on discrete strips the induced current to a single strip at a vertical distance \vec{a}_i from the starting point requires an integration along the strip (see Eq. (3)). The integration limits (x_i) have to be chosen depending on the area to be calculated.

$$\begin{aligned} I(\vec{r}_i) &= \int_{-x_i}^{x_i} \frac{1}{|\vec{a}_i|^2 + |\vec{x}_i|^2} dx_{1,i} = 2 \int_0^{x_i} \frac{1}{|\vec{a}_i|^2 + |\vec{x}_i|^2} dx_{1,i} \\ &= \frac{2}{|\vec{a}_i|} \arctan\left(\frac{|\vec{x}_i|}{|\vec{a}_i|}\right) \Big|_0^{x_i} = \frac{2}{a_i} \arctan\left(\frac{x_i}{a_i}\right) \end{aligned} \quad (3)$$

Contributing strips have to be summed up to derive the total amount of current within the chosen limits using Eq. (4).

$$I_{\text{Total}}(r) = \sum_{i=0}^n I(\vec{r}_i) \quad (4)$$

A simulation of 1 million particles with a random starting point within the source yielded the hit distribution shown in Fig. 4 (red line).

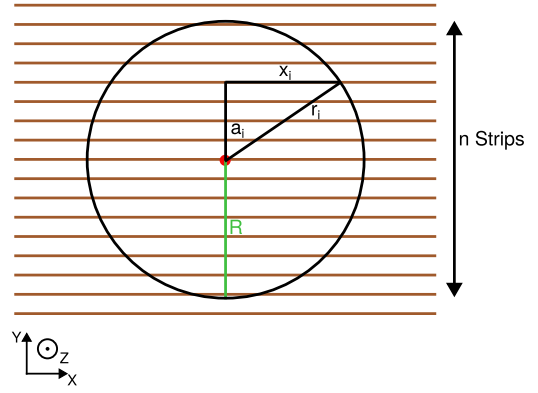


Fig. 3. Front view of the irradiation setup. To calculate the irradiation strength within a circle of radius R , all enclosed strips have to be taken into account. The intensity $I(\vec{r}_i)$ is integrated along the strip length x_i for each strip at a distance a_i from the starting position of the particle. The total intensity is derived by summing up all the individual intensities following Eq. (4).

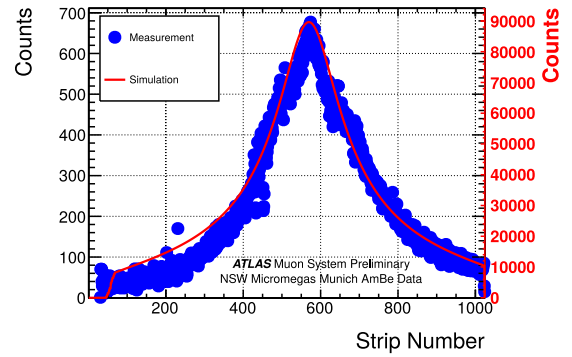


Fig. 4. Reconstructed cluster position of a random trigger measurement of SM2 irradiated by the Am-Be source. The red line is the simulated hit distribution of 1 million particles using Eq. (4). Good agreement is visible. Source: Figure taken from [8].

For comparison, a hit intensity measurement using a random trigger has been carried out. This actual measured hit distribution, given by the blue markers, shows an excellent agreement between simulation and measurement. A 2D expansion of the simulated hit distribution resulted in the relative intensity spectrum given in Fig. 5. The marked areas represent different values of HL-LHC equivalent interaction rates.

4. Long-term current behavior

The current drawn by the detector under irradiation has been monitored over three years. This current corresponds to the lower left sixth of the detector surface shown in Fig. 1. Over that period both gas mixtures have been tested. Currents for the Ar:CO₂ gas mixture and the 3.7 GBq AmBe source are shown in Fig. 6. A broad (± 40 nA) current spread, induced by neutrons, is observed.

For the ternary gas mixture, a narrower distribution is observed showing superior quenching capabilities (Fig. 7). During this irradiation period of 18 months a stronger 10 GBq source has been introduced. Multiple high voltage tests combined with additional tests after introducing the stronger source resulted in the irregularities observed around November 2021, where the current equals (0.1–0.5) μ A. However, no detector instabilities or discharges have been observed. Periods without current correspond to maintenance periods. Current fluctuations ($\Delta I = \mathcal{O}(0.1 \mu\text{A})$) correspond to environmental factors. Faster fluctuations ($f = \mathcal{O}(1 \text{ d}^{-1})$) result from pressure variations while a slow fluctuation with a frequency of 1 year⁻¹ originates from the seasonal temperature change between summer and winter.

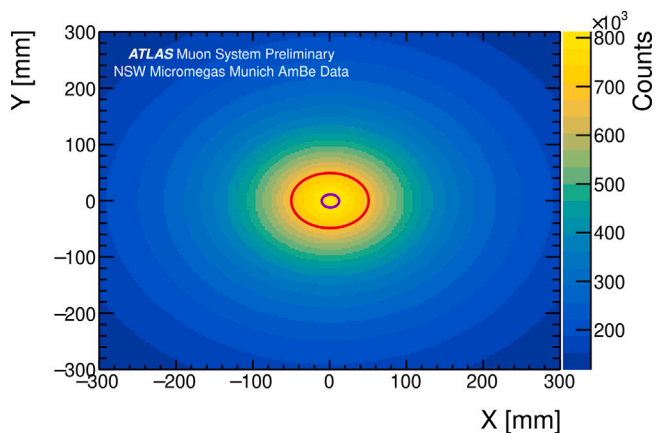


Fig. 5. Simulated 2D irradiation strength of the neutron source. The encircled areas correspond to HL-LHC equivalent irradiation strengths of 1xHL-LHC (red circle of $r=50$ mm) and 2.8xHL-LHC (purple circle of $r=5$ mm).
Source: Figure taken from [8].

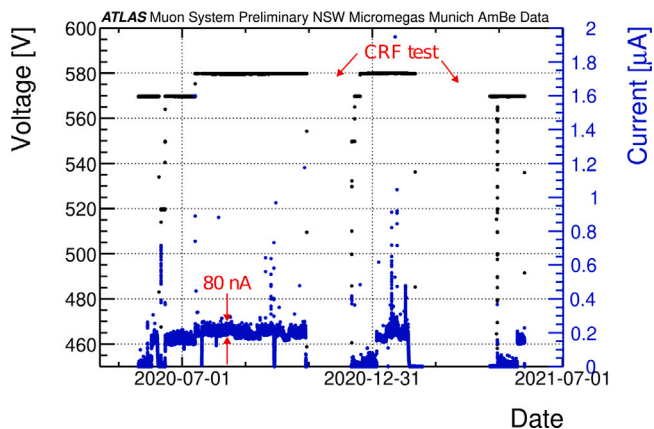


Fig. 6. One year of irradiation of the lower left sector of SM2 (see Fig. 1) under Ar:CO₂. A wide current spread of ± 40 nA originating from the neutron interaction in the detector and its corresponding secondary processes is visible. CRF denotes two intermediate test periods without irradiation not discussed in this paper, where zero current was drawn and hence no charge accumulated. Between the two test periods, the irradiation continued.
Source: Figure taken from [8].

5. Accumulated charge

Over the whole irradiation period a total of 0.011 C cm^{-2} has been accumulated (Fig. 8). Since this charge represents the whole area of the lower left sector of the detector (see Fig. 1), the value has to be scaled accordingly to the areas derived in Section 3. In these areas, only a fraction of the total charge is deposited, but due to the smaller area, the resulting accumulated charge per area increases. The fraction of the total accumulated charge follows by dividing the intensity of an area given by radius r by the total intensity of the detector, both derived from Eqs. (3) and (4). Scaling to the areas denoted in Fig. 5, 2 years and 5 years of HL-LHC equivalent were accumulated inside the red and purple area respectively.

This equivalent dose corresponds to the innermost region of the NSW and a hit intensity decrease with $1/r^{2.42}$ with radial distance r from the LHC beam pipe was observed [9].

6. Detector resolution

For performance measurements, the detector was investigated using cosmic muons. It was sandwiched between two scintillators, that were used in coincidence for triggering.

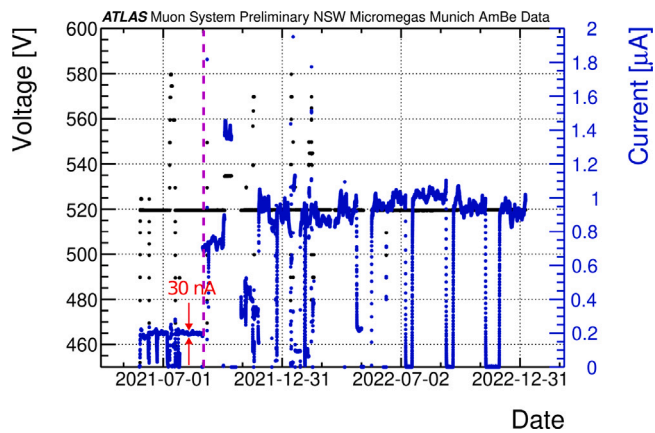


Fig. 7. 18 months of irradiation of the lower left sector of SM2 (see Fig. 1) under Ar:CO₂:iC₄H₁₀. The current fluctuations (± 15 nA) are much narrower compared to Fig. 6. This effect is best visible for the starting period where the 3.7 GBq AmBe source was used. No trips of the detector nor a clear decreasing trend hinting for less amplification due to aging is visible. The dips in the current are correlated to periods with no irradiation and service. The fluctuations in the current can be described by environmental fluctuations like pressure variations. A slow fluctuation with a frequency of $f = \mathcal{O}(1 \text{ year}^{-1})$ corresponds to seasonal temperature fluctuations between summer and winter. Current spikes, e.g. in January 2022 correspond to HV scans and not discharges.
Source: Figure taken from [8].

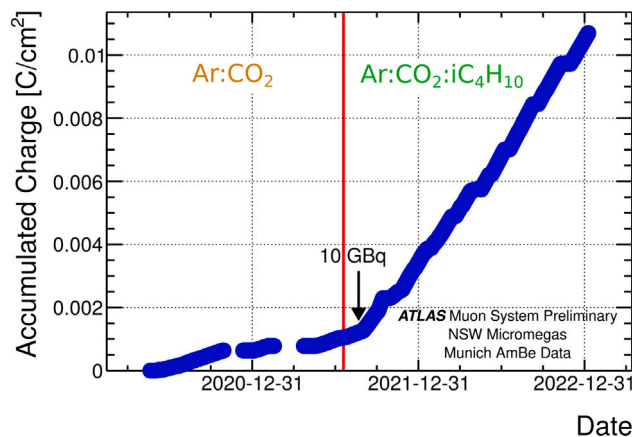


Fig. 8. Accumulated charge on the HV sector under irradiation. Indicated by the black arrow is the switch to the 10 GBq source resulting in a much steeper rise of the accumulated charge. The value shown represents the lower left detector section of Fig. 1 with an area of 2444.4 cm^2 . This has to be scaled accordingly for areas around the source center as shown in Fig. 5 resulting in multiple years of HL-LHC equivalent accumulated charges in the area closest to the center of irradiation.
Source: Figure taken from [8].

The detector resolution is determined by comparing the measured hit position in the detector with an expected hit position provided by the track determined by the other three detector layers. The difference is called residual and is sketched exemplarily in Fig. 9. The obtained distribution is fit by the sum of two Gaussian functions. Lastly, the finite track position estimation provided by the three other layers is taken into account. Comparing the resolution for different applied amplification voltages and the two gas mixtures shows the best resolutions for the ternary gas mixture at the highest amplification voltage of $U_{\text{Amp}} = 530 \text{ V}$ (see Fig. 10). These measurements were performed after three years of neutron irradiation using cosmic muons allowing track angles up to $\pm 26.5^\circ$.

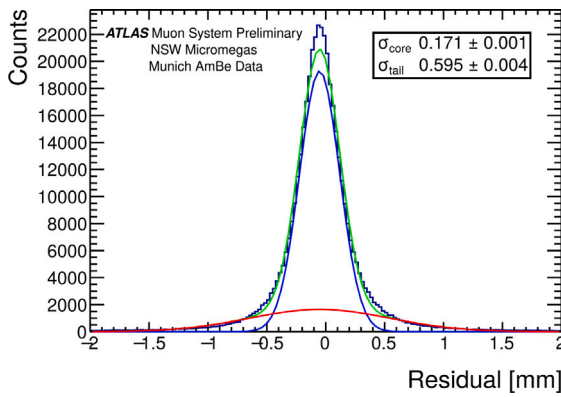


Fig. 9. Residual distribution obtained for cosmic muons allowing all particle tracks up to $\pm 26.5^\circ$. The distribution is fit by the sum of two Gaussians.

Source: Figure taken from [8].

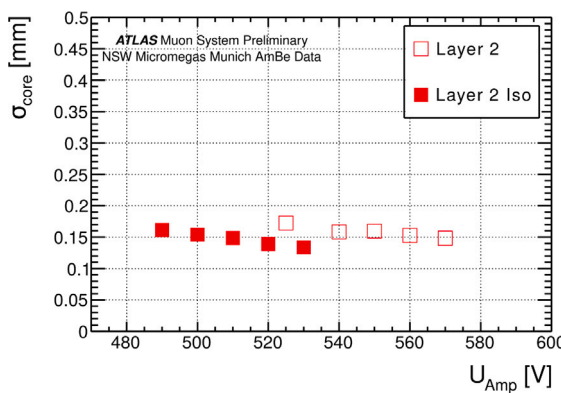


Fig. 10. Detector resolution obtained with cosmic muons allowing all particle tracks up to $\pm 26.5^\circ$. The label containing Iso corresponds to measurements using the ternary gas mixture.

Source: Figure taken from [8].

7. Efficiency

A particle reconstruction is counted as efficient if the residual lies within ± 5 mm of the track prediction. This number of efficient events is divided by the total number of events to determine the detector efficiency. For the two gas mixtures and various amplification voltages, the detector efficiency is displayed in Fig. 11. The expected increase with higher amplification voltages is observed with saturation at 98% for the ternary gas mixture at amplification voltages $U_{\text{Amp}} = 530$ V. This maximum efficiency is expected, resulting from structurally related inactive areas of the detector called interconnections [2].

The position-dependent efficiency of the most strongly irradiated sector is shown in Fig. 12. No decrease in efficiency around the source position (black cross) is observed. The inefficient area on the bottom right is the previously mentioned structurally related inactive area.

8. Summary

A spare NSW Micromegas module has been irradiated over three years by an AmBe neutron source. Two different gas mixtures have been tested (Ar:CO₂ 93:7 vol% and Ar:CO₂:iC₄H₁₀ 93:5:2 vol%). A characterization of the source has been performed and HL-LHC equivalent amounts of charges have been accumulated. Final performance tests after irradiation showed an efficiency well above the ATLAS design values of >90% [2]. In particular, in the area with the highest accumulated charge, no deterioration has been observed. No performance issues resulting from the change of the gas mixture are expected during the operation at ATLAS.

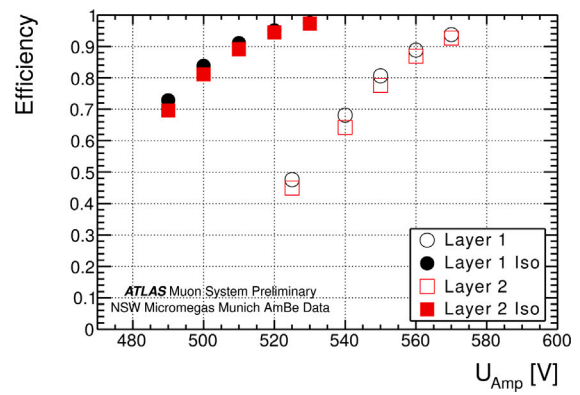


Fig. 11. Detector efficiency obtained with cosmic muons allowing all particle tracks up to $\pm 26.5^\circ$. The label containing Iso corresponds to measurements using the ternary gas mixture.

Source: Figure taken from [8].

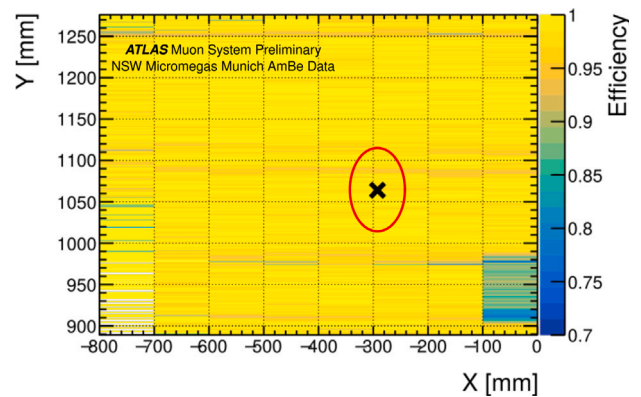


Fig. 12. Detector efficiency vs. position obtained with cosmic muons allowing all particle tracks up to $\pm 26.5^\circ$ after three years of irradiation. The black cross indicates the source position during irradiation. No decrease in efficiency in the vicinity of that position is observed. The drop in efficiency on the bottom right results from an insensitive region by construction (interconnections) [2].

Source: Figure taken from [8].

Declaration of competing interest

The authors declare that they have no known competing financial interests or personal relationships that could have appeared to influence the work reported in this paper.

Acknowledgments

This work is supported by the BMBF FSP-103 ErUM (Bundesministerium für Bildung und Forschung mit Forschungsschwerpunkt Erforschung von Universum und Materie).

References

- [1] I. Giomataris, P.C. Rebougeard, J.P. Robert, G. Charpak, Micromegas: a high-granularity position-sensitive gaseous detector for high particle-flux environments, Nucl. Instrum. Methods Phys. Res. A 376 (1995) 29–35, [http://dx.doi.org/10.1016/0168-9002\(96\)00175-1](http://dx.doi.org/10.1016/0168-9002(96)00175-1), 20 p. <http://cds.cern.ch/record/299159>.
- [2] ATLAS Collaboration, New small wheel technical design report, Tech. rep., ATLAS New Small Wheel Technical Design Report, 2013, <https://cds.cern.ch/record/1552862>.
- [3] F. Vogel, Test of ATLAS Micromegas detectors with ternary gas mixture at the CERN GIF++ facility, PoS EPS-HEP 2021 (2022) 757, <http://dx.doi.org/10.22323/1.398.0757>.

- [4] H. Basiri, H. Tavakoli-Anbaran, Investigation of some possible changes in am-be neutron source configuration in order to increase the thermal neutron flux using monte carlo code, *J. Phys. Conf. Ser.* 956 (1) (2018) 012010, <http://dx.doi.org/10.1088/1742-6596/956/1/012010>.
- [5] M. Winberg, R. Garcia, National low-level waste management program radionuclide report series, 14, 1995, <https://inis.iaea.org/collection/NCLCollectionStore/Public/27/032/27032341.pdf>.
- [6] J. Marion, J. Fowler, Fast neutron physics part 1, *Science* 132 (3427) (1960) 613–614, <http://dx.doi.org/10.1126/science.132.3427.613>, <https://www.science.org/doi/abs/10.1126/science.132.3427.613>.
- [7] S. Croft, The use of neutron intensity calibrated $^9\text{Be}(\alpha, n)$ sources as 4438 keV gamma-ray reference standards, *Nucl. Instrum. Methods Phys. Res. A* 281 (1) (1989) 103–116, [http://dx.doi.org/10.1016/0168-9002\(89\)91221-7](http://dx.doi.org/10.1016/0168-9002(89)91221-7).
- [8] ATLAS Muon System, GIF++ and LMU irradiation studies on ATLAS NSW Micromegas detectors, 2023, <https://atlas.web.cern.ch/Atlas/GROUPS/MUON/PLOTS/MDET-2023-10/>.
- [9] ATLAS Muon System, New small wheel performance plots based on 2022 data, Tech. rep., CERN, Geneva, 2023, <https://cds.cern.ch/record/2869618>.